Scientific Research Publishing

Journal of Materials Science and Chemical Engineering, 2024, 12, 49-60
https://www.scirp.org/journal/msce
ISSN Online: 2327-6053
ISSN Print: 2327-6045

Evaluation of Particle Properties of MgO/TiO_2 Material by Monte Carlo Simulation Method

Koffi N'guessan Placide Gabin Allangba[1,2,3*], Yves Kily Hervé Fagnidi[2,4], Hermann N'guessan[2], Zié Traoré[3,5], Koffi Arnaud Kamenan[2,6]

[1]Physics Pedagogical Unit, Laboratory of Environmental Science and Technology, University Jean Lorougnon Guédé, Daloa, Côte d'Ivoire
[2]Laboratory of Fundamental and Applied Physics, University Nangui Abrogoua, Abidjan, Côte d'Ivoire
[3]Department of Medical Physics, University of Trieste and International Centre for Theoretical Physics (ICTP), Trieste, Italy
[4]Department of Science and Technology, University Alassane Ouattara, Bouaké, Côte d'Ivoire
[5]Nuclear Physics and Radiation Protection Team, Laboratory of Material Sciences Environment and Solar Energy, University Felix Houphouet-Boigny, Abidjan, Côte d'Ivoire
[6]Department of Mathematics, Physics and Chemistry, UFR Biological Sciences, University Peleforo Gon Coulibaly, Korhogo, Côte d'Ivoire
Email: *pgallangba@gmail.com

How to cite this paper: Allangba, K.N.P.G., Fagnidi, Y.K.H., N'guessan, H., Traoré, Z. and Kamenan, K.A. (2024) Evaluation of Particle Properties of MgO/TiO_2 Material by Monte Carlo Simulation Method. *Journal of Materials Science and Chemical Engineering*, **12**, 49-60.
https://doi.org/10.4236/msce.2024.122004

Received: January 9, 2024
Accepted: February 19, 2024
Published: February 22, 2024

Copyright © 2024 by author(s) and Scientific Research Publishing Inc.
This work is licensed under the Creative Commons Attribution International License (CC BY 4.0).
http://creativecommons.org/licenses/by/4.0/
Open Access

Abstract

The simulation by the Monte Carlo method executed by the software PyPENELOPE proved effective to specify the particle propagation characteristics by calculating the absorption fractions, backscattering and transmission of electrons and secondary photons under the incidence of 0.5 to 20 KeV range of primary electrons. More than 99.9% of the primary electrons were transmitted in the 125 nm thick MgO/TiO_2 material at 20 KeV. This occurred because several interactions took place in the transmitted primary irradiation such as characteristic, fluorescence, and bremsstrahlung produced when of the occupation of the KL3, KL2, KM3, and KM2 shell and sub-shell of titanium and magnesium which are the elements with a high atomic number in the material. The transmission particle characteristic of this material is therefore an indicator capable of improving the electrical performance and properties of the sensor.

Keywords

Monte Carlo, PyPENELOPE, Primary Electrons Transmission, MgO/TiO_2

1. Introduction

Because of the great technological interest of applications in nanoscience, many research works both by experimentation and simulation have been conducted to elucidate the mechanism of understanding the trajectory of electrons and photons revealing the electronic and optical properties of certains nanomaterials doped thin oxide such as titanium oxide (TiO_2) and magnesium monoxide (MgO). TiO_2 is one of the most widely used nanomaterials in a wide range of applications, including as a white pigment for the pharmaceutical and food industry, skin sunscreen, photo-catalysts [1] [2], water treatment, hydrogen production, ethylene recovery and antimicrobial activity [3] [4] [5] [6] [7]. One of the major problems with TiO_2 is that the extent of electron hole recombination is higher than that of some other promising materials [8]. In an attempt to overcome this problem, researchers are implementing many ways to improve the solar conversion efficiency of TiO_2 while using doping studies [9]. Metal oxides are recognized as the best TiO_2 dopants. The most common that has been synthesized into a range of nanostructure morphologies is MgO. It is known as an inert material with a high melting point, as a typical wide band-gap insulator. And its substrate has been widely used for high-Tc superconductor (HTSC) thin-film coating applications worldwide. When it is used as a substrate for nanoparticle catalysts, the main physical properties need to be better understood for the transition from solid state to molecule scale [10]. Impressive results in medical biotechnology indicated that the TiO_2 nano-thin film coating stimulated the adhesion and proliferation of coronary arterial endothelial cells with additional characteristics acting as a protective barrier [11]. The data revealed that surface morphology and surface hydrophilia contributed to the success of the atomic layer deposition nanoscale coating, which also acted as a protective layer inhibiting the release of harmful degradation products from the magnesium-zinc stent [11]. Based on the studies of Luis Anaya *et al.*, mixed oxide nanoparticles (MONs, TiO_2-ZnO-MgO) obtained by the sol-gel method were characterized by transmission electron microscopy and thermogravimetric analysis. In addition, the effect of MON on the microbial growth of *Escherichia coli*, *Salmonella paratyphi*, *Staphylococcus aureus,* and *Listeria monocytogenes*, as well as the toxicity against Artemia salina by the lethal concentration test was evaluated [12]. Several research teams have also printed thin films to study the experimental physical properties of materials [13]. This study can be carried out thanks to the Monte Carlo (MC) simulation method which is used because of its high accuracy such as Gamma ray transport [14]. MC was used to reduce the complexity of mathematical expressions in which Fourier random characteristics are applied to approach the Exponentiated Quadratic kernel [15]. It is possible to simulate certains phenomena such as the cascade of particles in materials of Novel lead oxide-based flexible dosimeters for electron therapy [16] [17]. Monte Carlo simulation is a crucial tool for specifying the possible density of dispersed particles, the generation of secondary radiation, and the transmission ratio of primary particles from the material structure. Various simulation software, including Geant4, MCNPX, and PyPENELOPE, were composed to simulate the interactions between the particles and the designed structure. Most of these simulation programs depend on multiple scattering theories for electron transport to reduce computation time [18]. PENELOPE means Penetration and energy loss of positrons and electrons in matter. It uses the Monte Carlo method for the simulation of numerous apparatuses as dosimeter and material structure. It will therefore be a tool of choice to simulate MgO/TiO_2. PENELOPE combines numerical and analytical total and differential cross sections (DCS) to describe the different interaction mechanisms. These cross-sections are the result of approximate physical models and, therefore, are affected by systematic uncertainties. The interaction mechanisms considered in PENELOPE, and the corresponding DCSs, are as follows: Elastic diffusion of electrons and positrons where these cross sections were calculated using the program ELSEPA [19], Inelastic collisions of electrons and positrons [20] [21], Electron impact ionization [22], Bremsstrahlung emission by electrons and positrons [23] [24] [25], Positron annihilation, Coherent dispersion (Rayleigh) of photons, Incoherent dispersion (Compton) of photons [26], Photoelectric absorption of photons [27], Production of electron-positron pairs [28]. Buse *et al*. conducted a study on the structural, morphological and optical properties and performance of gas sensors of titanium dioxide (TiO_2) doped thin films with magnesium oxide (MgO). The material was therefore manufactured in different thicknesses namely 125 nm, 140 nm and 190 nm. The best results obtained with the material of thickness 125 nm. They showed that the dopant is able to improve the electrical performance and properties of the sensor [29]. In our work, we will attempt to provide additional information on particle properties in order to explain the microscopic electron propagation in MgO/TiO_2.

2. Materials and Methods

This work was performed with Monte Carlo simulation code using the PyPENELOPE software which is a version of PENELOPE executed by the Python program as was the case in several works [30] [31] [32] [33] [34]. It is one of the best tools to evaluate the transport of the particle in the material describing the different types of interaction. The material MgO/TiO_2 studied by Buse *et al*. which presented certain physical properties but without giving the characteristics of particle propagation related to the absorption, backscattering and transmission properties of electrons and photons in matter. In this work, we simulated a primary electron incident beam and sent perpendicularly on the MgO/TiO_2 material in the optimal conditions in order to study the propagation effects. Our beam source was at the initial coordinate position (0; 0; 0) under a polar angle range of zero to 180˚. The number of electrons was a range from 7.5×10^6 to 26.3×10^6. The diameter of the beam was set to 10 μm. Multilayer geometry was used for the material consisting of MgO density 3.35 g/cm^3 and TiO_2 density 4.23 g/cm^3. The default interaction forcing was configured and used during the simulation. These simulations were performed for different values of incident irradiation of range 0.5 KeV to 20 KeV. The work of Buse *et al.* showed the 125 nm thickness material is promising for the sensor fabricator [29]. It will therefore be the subject of our study. Each molecule composing the material was half the total thickness *i.e.*, 62.5 nm for MgO and 62.5 nm for TiO_2. A laptop computer performed the simulation with i5 2.4 GHz CPU and 8 GB RAM under Windows operating systems. The PyPENELOPE software simulation parameters were defined as in **Table 1** [35].

3. Results and Discussion

Many research teams studied the MgO/TiO_2 material to understand its geometrical structure, electronic structure, and other general interfacial properties, which are not yet clear from a microscopic perspective. In this work, the MgO/TiO_2 thickness proposed by Buse *et al.* was 125 nm. **Table 2** below presents the results of simulations relating to the fraction of particles absorbed, backscattered or transmitted in the material according to the different beam energies.

The fractions of absorbed, backscattered and transmitted radiation within MgO/TiO_2 structure were obtained after simulating a number of electrons ranging from 7.5×10^6 to 26.3×10^6 and their distributions were estimated via the pyPENELOPE Monte Carlo code. Our study is focused on the propagation effect of a range of 0.1 KeV to 20 KeV of incident primary irradiation on 125 nm as thickness of MgO/TiO_2 materials. Absorbed fraction for primary irradiation spread on a range of 1.484×10^{-5} to 0.8133 on all the energy. It decreases to the smallest value except for secondary electron which increases to a peak at 5 KeV before decreasing to 10 KeV (**Figure 1(a)**). Regarding backscattered fraction, Primary irradiation fraction is high for small incident beam energy. **Figure 1(b)** show the plots decrease when the energy increase. Regarding the transmitted fraction, almost all incident primary beam was transmitted when the energies increase. **Figure 1(c)** shows from 0.5 to 10 KeV a growing right and after 10 KeV up to 20 KeV, a plateau whose constituent points vary very little keeping a transmission fraction ranging from 93 to 99.9% within material. Uncertainty is low for all calculation (**Table 2**). The transmission fraction is acceptable because its agreement with Senol's works [16]. The highest energy gives therefore a better transmitted fraction.

Table 1. Simulation parameters.

Material	Absorption energy of electrons (eV)	Absorption energy of photons (eV)	Absorption energy of positrons (eV)	Elastic scattering parameter C1	Elastic scattering parameter C2	Cutoff energy loss of inelastic collision-WCC (eV)	Cutoff energy loss of Bremsstrahlung collision-WCR (eV)
MgO	50.0	50.0	50.0	0.2	0.2	50.0	50.0
TiO_2	50.0	50.0	50.0	0.2	0.2	50.0	50.0

Table 2. Absorbed, backscattered and transmitted fraction of the simulated primary and secondary irradiations.

MgO/TiO_2	Primary irradiation		Secondary electron		Secondary photon	
	Fraction	Uncertainty $\times 10^{-5}$	Fraction	Uncertainty $\times 10^{-5}$	Fraction	Uncertainty $\times 10^{-5}$
0.5 KeV						
Absorbed	0.8133	34.54	1.05	77.28	1.956×10^{-5}	8.872×10^{-4}
Backscattered	0.2061	47.02	0.01945	12.48	1.381×10^{-5}	7.571×10^{-4}
Transmitted	4.613×10^{-9}	5.639×10^{-6}	4.613×10^{-9}	5.639×10^{-6}	1.455×10^{-5}	1.201×10^{-4}
1 KeV						
Absorbed	0.8337	39.63	2.633	150.6	6.017×10^{-5}	5.729×10^{-2}
Backscattered	0.1864	54.81	0.02011	15.18	4.21×10^{-5}	7.032×10^{-2}
Transmitted	9.335×10^{-8}	4.881×10^{-8}	9.335×10^{-8}	4.881×10^{-3}	1.092×10^{-5}	4.265×10^{-2}
5 KeV						
Absorbed	0.4713	79.49	12.17	1038	0.0007582	91.55
Backscattered	0.1642	75.28	0.01341	18.29	0.000582	1.11
Transmitted	0.393	96.7	0.01503	19.48	0.0005472	91.01
10 KeV						
Absorbed	0.0101	8.382	4.573	438.8	0.0003839	49.35
Backscattered	0.08545	29.95	0.008214	7.564	0.0003717	62.78
Transmitted	0.9332	35.68	0.02055	12.01	0.0003786	52.46
15 KeV						
Absorbed	0.0002819	98.13	2.581	182.6	0.0002335	33.36
Backscattered	0.03223	13.79	0.005595	4.376	0.0002493	43.27
Transmitted	0.9879	16.58	0.01486	7.116	0.0002623	36.53
20 KeV						
Absorbed	1.484×10^{-5}	42.06	1.809	257.5	0.0001696	61.04
Backscattered	0.01648	19.23	0.004446	7.32	0.0001922	80.83
Transmitted	0.9996	23.67	0.01161	11.76	0.0002046	67.23

The probability density of backscattered and transmitted particles distributed according to the energy in the material of 125 nm, is illustrated in the following Figure 1 and Figure 2.

For incident primary irradiation of 20 KeV, the energy distribution of the backscattered electrons extends over a range from zero to 20 KeV. A peak of the probability density just after 0 KeV is observed and decreases immediately before increasing again for another peak around 18 KeV. After this peak, the probability again reaches another peak at 20 KeV. This shows that the primary electrons propagate in cascade by penetrating in the structure of the material thus creating interactions with the electrons present on the transitions of the

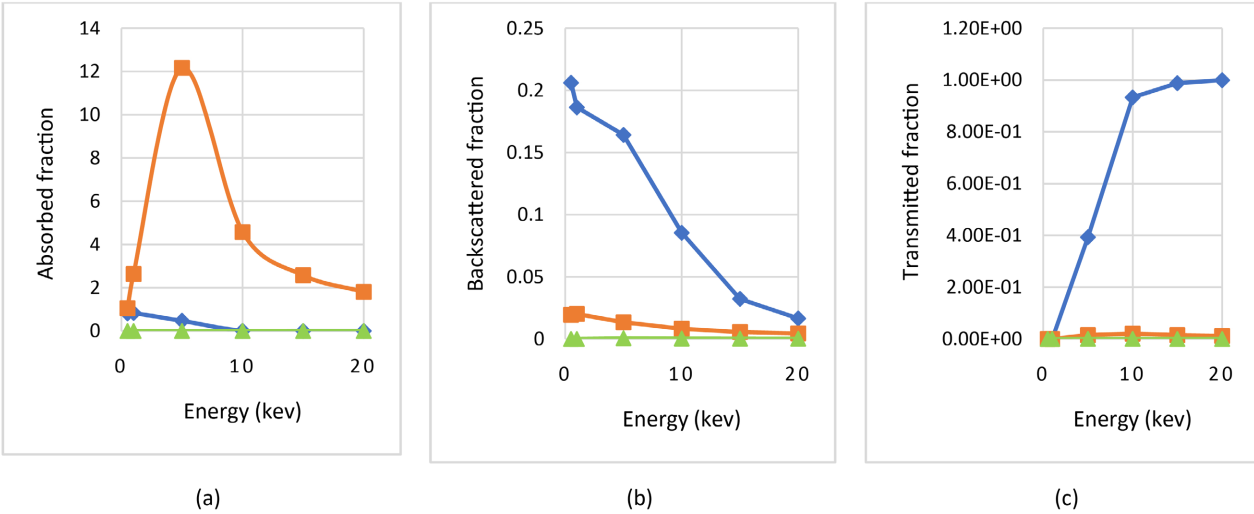

Figure 1. Primary irradiation (in blue line), secondary electron (in orange line), secondary photon (in green line), absorbed fraction (a), backscattered fraction (b), transmitted fraction (c).

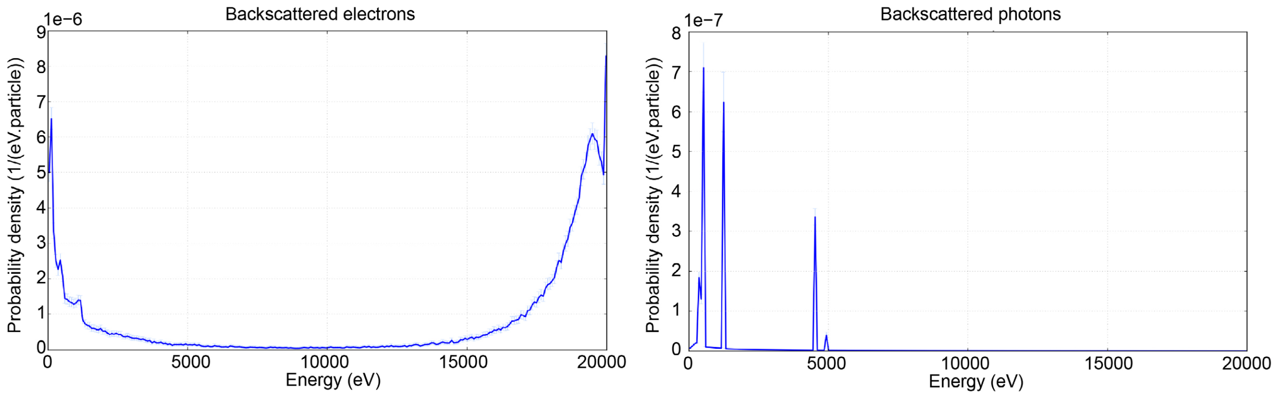

Figure 2. Backscattered electrons and photons energy distribution in the MgO/TiO_2 material at 20 KeV.

atomic elements constituting the material. Thus, a low probability density of electrons and photons is evidenced. The backscattered photons weakly emit two signals in peak before 1 KeV, a peak at about 1.2 KeV and a peak between 4 and 5 KeV (**Figure 2**). A similar phenomenon is also observed for transmitted photons (**Figure 3**). Concerning transmitted electrons, a density of probability almost zero during the simulation and begins to increase from 17 KeV and reaches a peak around 19 KeV (**Figure 3**).

The polar angle changes from 0 to 180˚ during the simulation. The probability density started to increase to 120˚ for emerging electrons and reach a peak at 180˚. Emerging photon probability density is stable during simulation from 0 to 180˚ but drop only in 90˚ (**Figure 4**).

The peaks observed then of emission and backscattering of the particles also appear on **Figure 5(a)** of the photon spectrum.The curve described by the photon spectrum is Bremsstrahlung phenomenon. It occurred on all energy range (**Figure 5**).

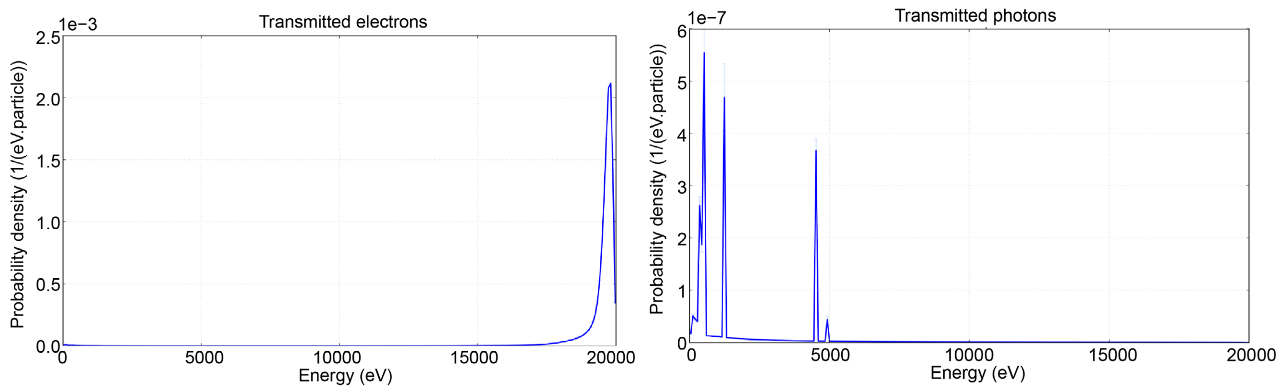

Figure 3. Transmitted electrons and photons energy distribution in the MgO/TiO_2 material at 20 KeV.

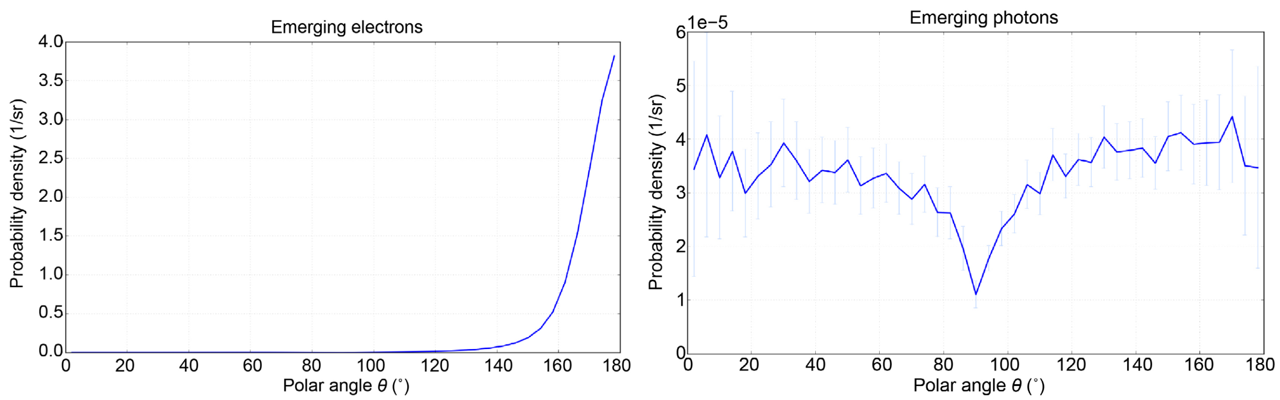

Figure 4. Polar angle dependency of emerging photons and electrons emitted from MgO/TiO_2 material with 125 nm thickness.

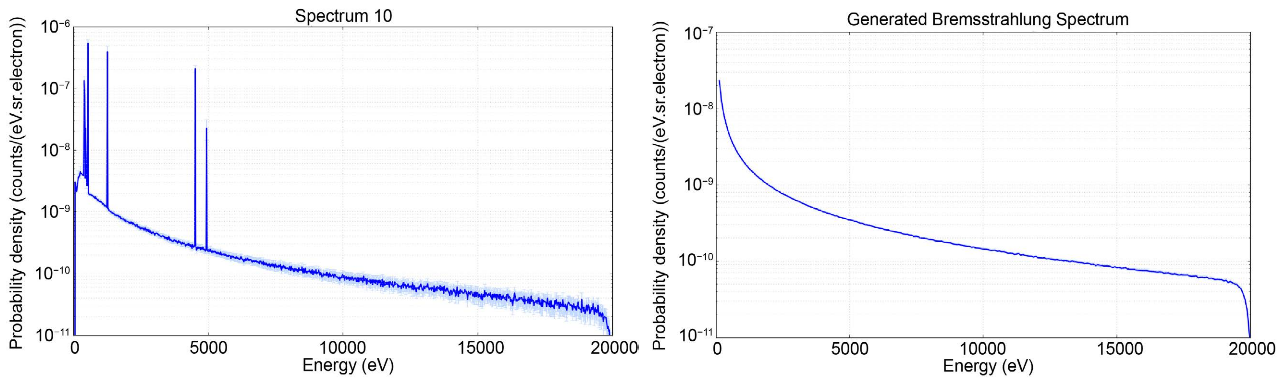

Figure 5. Photon spectrum (a) and bremsstrahlung spectrum (b).

Figure 6 showed that the characteristic energy of titanium (Z = 22) electron transitions is between 4 and 5 KeV. These lines are very different, we can quote KL3, KL2, KM3 and KM2 sub-shell occupied under certain incident energy like 10 and 20 KeV. Typically, Kβ line of Ti is 4.931 KeV [36]. Kα line of Mg (1.253 KeV) [37] is higher than 1 KeV, it is therefore not shown in **Figure 6(c)**. The particle occupation of these titanium and magnesium shell and sub-shell are responsible for the better transmission fraction rate of primary electrons in the material and cause the phenomena such as the emission of characteristics,

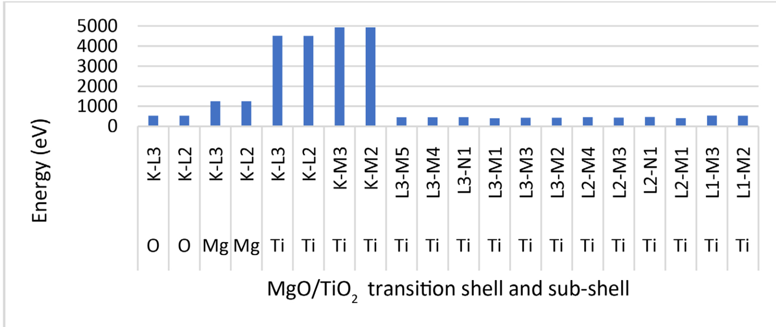

(a)

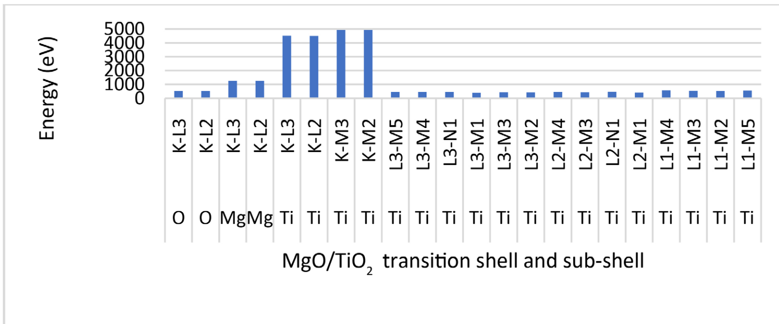

(b)

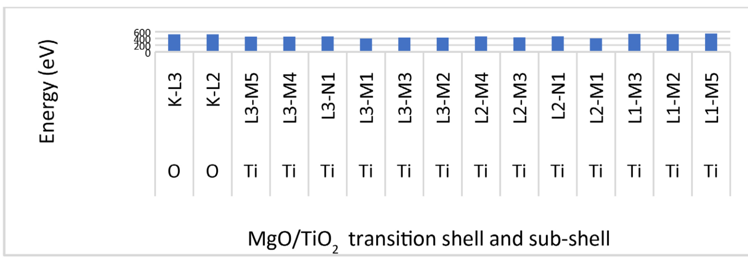

(c)

Figure 6. Transition shell and sub-shell energy Histogram at 20 KeV (a), 10 KeV (b) and 1 KeV (c) incidence primary irradiation beam in MgO/TiO_2 material.

fluorescence X-rays and bremsstrahlung. At low incidence energy (1 KeV), the particle occupancy of these shell and sub-shell is low and non-existent in magnesium (**Figure 6(c)**). Indeed, these high-energy electrons must release energy to fill the lower energy gaps in the atom. These generated photons can be classified as radiation contamination for sensor application. Therefore, potential radiation contamination consists of generated X-rays, including the continuum (Bremsstrahlung), X-ray characteristics and fluorescence [38].

4. Conclusion

At the end of this study, it was demonstrated the good quality of the Monte Carlo simulation method by the PyPENELOPE software which was revealed to be a tool of choice in the calculation of the absorption, backscatter and transmission fraction of particles through the material. Under an incident energy of 20 KeV of primary electrons, more than 99.9% of these particles were transmitted in the material MgO/TiO_2 thanks to several radiation interaction matter which governs this particle propagation namely the characteristic line, fluorescence and bremsstrahlung. These interactions were produced on KL3, KL2, KM3, and KM2 shell and sub-shell of Mg and Ti. These properties may therefore improve the performance of this material in the manufacture of future sensors.

Acknowledgement

The study was performed by Medical Physics research unit in Côte d'Ivoire, ICTP, Trieste University in Italy. The authors acknowledge with gratitude the support from the unit.

Conflicts of Interest

The authors declare no conflicts of interest regarding the publication of this paper.

References

[1] Hoffmann, M.R., Martin, S.T., Choi, W. and Bahnemann, D.W. (1995) Environmental Applications of Semiconductor Photocatalysis. *Chemical Reviews*, **95**, 69-96. https://doi.org/10.1021/cr00033a004

[2] Linsebigler, A.L., Lu, G.Q. and Yates Jr., J.T. (1997) Photocatalysis on TiO_2 Surfaces: Principles, Mechanisms, and Selected Results. *Chemical Reviews*, **95**, 735-738. https://doi.org/10.1021/cr00035a013

[3] Venkatasubramanian, R., Srivastava, R.S. and Misra, R.D.K. (2008) Comparative Study of Antimicrobial and Photocatalytic Activity in Titania Encapsulated Composite Nanoparticles with Different Dopants. *Materials Science and Technology*, **24**, 589-595. https://doi.org/10.1179/174328408X282065

[4] Robichaud, C.O., Uyar, A.E., Darby, M.R., Zucker, L.G. and Wiesner, M.R. (2009) Estimates of Upper Bounds and Trends in Nano-TiO_2 Production as a Basis for Exposure Assessment. *Environmental Science & Technology*, **43**, 4227-4233. https://doi.org/10.1021/es8032549

[5] Pérez-Larios, A., Hernandez-Gordillo, A., Morales-Mendoza, G., Lartundo-Rojas, L., Mantilla, A. and Gómez, R. (2016) Enhancing the H_2 Evolution from Water-Methanol Solution Using Mn^{2+}-Mn^{+3}-Mn^{4+}Redox Species of Mn-Doped TiO_2 Sol-Gel. *Catalysis Today*, **266**, 9-16. https://doi.org/10.1016/j.cattod.2015.12.029

[6] Anaya-Esparza, L.M., Ruvalcaba-Gómez, J.M., Romero-Toledo, R., Sánchez-Burgos, J.A., Montalvo-González, E. and Pérez-Larios, A. (2021) Investigating Structural Changes of Chitosan-TiO_2 and Chitosan-TiO_2-ZnO-MgO Hybrid Films during Storage by FTIR Spectroscopy. *Macedonian Journal of Chemistry and Chemical Engineering*, **40**,197-211. https://doi.org/10.20450/mjcce.2021.2396

[7] Roychaudhury, A.M., Utsa, D., Sujay, M., Goutam, K.B., Abhigyan D., Masanta, S., Achintya S., Aritra B., Debtanu G., Partha, C. and Apurba, K.D. (2022) Synthesis Structural and Anti-Microbial Characterization of Nanostructured Doped Tin Oxide. *Journal of Theoretical and Applied Physics*, **16**, Article ID: 162202.

[8] Fujishima, A. and Honda, K. (1972) Electrochemical Photolysis of Water at a Semi-

conductor Electrode. *Nature*, **238**, 37-38. https://doi.org/10.1038/238037a0

[9] Li, X., Huang, H., Bin, H., Peng, Z., Zhu, C., Xue, L., Zhang, Z.G., Zhang, Z., Ade, H. and Li, Y. (2017) Synthesis and Photovoltaic Properties of a Series of Narrow Bandgap Organic Semiconductor Acceptors with Their Absorption Edge Reaching 900 nm. *Chemistry of Materials*, **29**, 10130-10138. https://doi.org/10.1021/acs.chemmater.7b03928

[10] Liang, C., Can, X., Zhang, X.F. and Tao, Z. (2009) Raman and Infrared-Active Modes in MgO Nanotubes. *Physica E*: *Low-Dimensional Systems and Nanostructures*, **41**, 852-855. https://doi.org/10.1016/j.physe.2009.01.006

[11] Fan, Y., Run. C. and Webster, T.J. (2019) Atomic Layer Deposition Coating of TiO_2 Nano-Thin Films on Magnesium-Zinc Alloys to Enhance Cytocompatibility for Bioresorbable Vascular Stents. *International Journal of Nanomedicine*, **14**, 9955-9970. https://doi.org/10.2147/IJN.S199093

[12] Anaya-Esparza, L.M., González-Silva, N., Yahia, E.M., González-Vargas, O.A., Montalvo-González, E. and Pérez-Larios, A. (2019) Effect of TiO_2-ZnO-MgO Mixed Oxide on Microbial Growth and Toxicity against *Artemia salina*. *Nanomaterials*, **9**, Article 992. https://doi.org/10.3390/nano9070992

[13] Jun, S.C., Dong, W.K., Jun, Y.S., Jae, H.N. and Ji, H.C. (2020) Electrical and Chemical Sensing Properties of a Printed Indium-Tin-Oxide Film for the Detection of Hazardous and Noxious Substances. *Journal of the Korean Physical Society*, **76**, 1005-1009. https://doi.org/10.3938/jkps.76.1005

[14] El-Tayebany, R.A. and Elbegawy, H. (2023) Assessment of Modeling Collimator Designs for γ-Ray Transmission of Uranium Oxide Spectrometry Using HPGe Detectors. *World Journal of Engineering and Technology*, **11**, 663-671. https://doi.org/10.4236/wjet.2023.114044

[15] Di, Q.L. (2022) Quasi-Monte Carlo Approximations for Exponentiated Quadratic Kernel in Latent Force Models. *Open Journal of Modelling and Simulation*, **10**, 349-390. https://doi.org/10.4236/ojmsi.2022.104021

[16] Senol, K. (2022) An Investigation on Quantitative Detector Characteristics of Novel Flexible Skin Dosimeter Using Monte Carlo Simulation Method. *Journal of New Results in Science*, **11**, 100-110. https://doi.org/10.54187/jnrs.1103993

[17] Michael, S., Tara, N., Genevieve, N.H., Bradley, W., Jérémie, W., Bjoern, N., Christophe, B., Volker R., David, P.F. and Mariana, I.B. (2017) Charge Collection in Hybrid Perovskite Solar Cells: Relation to the Nanoscale Elemental Distribution. *IEEE Journal of Photovoltaics*, **7**, 590-597. https://doi.org/10.1109/JPHOTOV.2016.2633801

[18] Kahraman, A., Kaya, S., Jaksic, A. and Yilmaz, E. (2015) A Comprehensive Study on the Photon Energy Response of RadFET Dosimeters Using the PENELOPE Monte Carlo Code. *Radiation Effects and Defects in Solids*, **170**, 367-376. https://doi.org/10.1080/10420150.2015.1010167

[19] Salvat, F., Jablonski, A. and Powell, C. (2005) ELSEPA-Dirac Partial-Wave Calculation of Elastic Scattering of Electrons and Positrons by Atoms, Positive Ions and Molecules. *Computer Physics Communications*, **165**, 157-190. https://doi.org/10.1016/j.cpc.2004.09.006

[20] Liljequist, D. (1983) A Simple Calculation of Inelastic Mean Free Path and Stopping Power for 50 eV-50 keV Electrons in Solids. *Journal of Physics D*: *Applied Physics*, **16**, 1567-1582. https://doi.org/10.1088/0022-3727/16/8/023

[21] Sternheimer, R. (1952) The Density Effect for the Ionization Loss in Various Materials. *Physical Review Journals Archive*, **88**, 851-859.

https://doi.org/10.1103/PhysRev.88.851

[22] Bote, D. and Salvat, F. (2008) Calculations of Inner-Shell Ionization by Electron Impact with the Distorted-Wave and Plane-Wave Born Approximations. *Physical Review A*, **77**, Article ID: 042701. https://doi.org/10.1103/PhysRevA.77.042701

[23] Acosta, E., Llovet, X. and Salvat, F. (2002) Monte Carlo Simulation of Bremsstrahlung Emission by Electrons. *Applied Physics Letters*, **80**, 3228-3330. https://doi.org/10.1063/1.1473684

[24] Kissel, L., Quarles, C. and Pratt, R. (1983) Shape Functions for Atomic-Field Bremsstrahlung from Electrons of Kinetic Energy 1-500 keV on Selected Neutral Atoms 1 ≤ Z ≤ 92. *Atomic Data and Nuclear Data Tables*, **28**, 381-460. https://doi.org/10.1016/0092-640X(83)90001-3

[25] Brusa, D., Stutz, G., Riveros, J., Fernández-Vera, J. and Salvat, F. (1996) Fast Sampling Algorithm for the Simulation of Photon Compton Scattering. *Nuclear Instruments and Methods in Physics Research Section A*: *Accelerators*, *Spectrometers*, *Detectors and Associated Equipment*, **379**, 167-175. https://doi.org/10.1016/0168-9002(96)00652-3

[26] Cullen, D.E., Chen, M.H., Hubbell, J.H., Perkins, S.T., Plechaty, E.F., Rathkopf, J.A. and Scofield, J.H. (1989) Tables and Graphs of Photon-Interaction cross Sections from 10 eV to 100 GeV Derived from the LLNL Evaluated Photon Data Library (EPDL). Lawrence Livermore National Laboratory (LLNL), Livermore. https://doi.org/10.2172/6901925

[27] Berger, M. and Hubbell, J. (1987) Photon cross Sections on a Personal Computer. National Bureau of Standards, Washington DC. https://doi.org/10.2172/6016002

[28] Perkins, S., Cullen, D., Hubbell, J., Rathkopf, J. and Scofield, J. (1991) Tables and Graphs of Atomic Subshell and Relaxation Data Derived from the LLNL Evaluated Atomic Data Library (EADL), Z=1-100. Lawrence Livermore National Lab. (LLNL), Livermore. https://doi.org/10.2172/10121422

[29] Buse, C.S., Nihan, A.S., Meltem, D.K. and Suleyman, O. (2019) Development of MgO: TiO_2 Thin Films for Gas Sensor Applications. *Ceramics International*, **45**, 2917-2921. https://doi.org/10.1016/j.ceramint.2018.11.079

[30] Stewart, R.D., Wilson, W.E., McDonald, J.C. and Strom, D.J. (2002) Microdosimetric Properties of Ionizing Electrons in Water: A Test of the PENELOPE Code System. *Physics in Medicine and Biology*, **47**, 79-88. https://doi.org/10.1088/0031-9155/47/1/306

[31] Requena, S., Williams, S. and Quarles, C.A. (2010) A Comparison of the Bremsstrahlung Yields from 53 keV Electrons on Gold Targets Produced by PENELOPE and Experiment. *Nuclear Instruments and Methods in Physics Research Section B*: *Beam Interactions with Materials and Atoms*, **268**, 3561-3568. https://doi.org/10.1016/j.nimb.2010.09.006

[32] Gonzales, D., Cavness, B. and Williams, S. (2011) Angular Distribution of Thick-Target Bremsstrahlung Produced by Electrons with Initial Energies Ranging from 10 to 20 keV Incident on Ag. *Physical Review A*, **84**, Article ID: 052726. https://doi.org/10.1103/PhysRevA.84.052726

[33] Statham, P., Llovet, X. and Duncumb, P. (2012) Systematic Discrepancies in Monte Carlo Predictions of k-Ratios Emitted from Thin Films on Substrates. *IOP Conference Series*: *Materials Science and Engineering*, **32**, Article ID: 012024.

[34] Adamson, P., Cannon, C. and Williams, S. (2021) Bremsstrahlung Produced by 5 keV Electrons Incident on BeO and NaCl. *Nuclear Instruments & Methods in Physics Research Section B*: *Beam Interactions with Materials and Atoms*, **490**,

43-47. https://doi.org/10.1016/j.nimb.2021.01.006

[35] Yi, C.Y., Hah, S.H. and Yeom, M.S. (2006) Monte Carlo Calculation of the Ionisation Chamber Response to Co-60 Beam Using PENELOPE. *Medical Physics*, **33**, 1213-1221. https://doi.org/10.1118/1.2188822

[36] Camus, P. (2009) Thermo Scientific. White Paper 51782.

[37] Hyperphysics Concept (2023) Experimental K α X-Rays Energies. http://hyperphysics.phy-astr.gsu.edu/hbase/Tables/kxray.html

[38] Sangeetha, P., Divya, K.N., Sandhya, B. and Subrahmanya, B.B. (2020) Production of X-RAYS Using X-RAY Tube. *Journal of Physics*: *Conference Series*, **171**2, Article ID: 012036.